



## Research paper

# A vacuum ultraviolet photoionization study on oxidation of JP-10 (*exo*-Tetrahydrodicyclopentadiene)



Long Zhao<sup>a</sup>, Weiye Chen<sup>b</sup>, Huaijiang Su<sup>c</sup>, Jiuzhong Yang<sup>b</sup>, Ralf I. Kaiser<sup>a,\*</sup>

<sup>a</sup> Department of Chemistry, University of Hawaii at Manoa, Honolulu, HI 96822, USA

<sup>b</sup> National Synchrotron Radiation Laboratory, University of Science and Technology of China, Hefei, Anhui 230029, China

<sup>c</sup> College of Mechanical Engineering, Guangxi University, Nanning, Guangxi 530004, China

## HIGHLIGHTS

- An experimental study was performed to unravel the high-temperature oxidation of JP-10.
- The products were identified *in situ* via VUV photoionization with mass spectroscopic detection.
- In the oxidation of JP-10, 62 species – among them 25 oxygenated molecules – were identified.
- The oxygenated species might be formed from the oxidation of the hydrocarbon intermediates.

## ABSTRACT

We conducted an experimental study to unravel the oxidation of tricyclo[5.2.1.0<sup>2,6</sup>]decane (JP-10) utilizing a high-temperature flow tube reactor over a temperature range of 900 K to 1031 K and the pressure of 600 Torr with the residence times of  $120 \pm 20$  ms. The products were identified *in-situ* in a supersonic molecular beam via single photon vacuum ultraviolet (VUV) photoionization coupled with mass spectroscopic detection in a reflectron time-of-flight mass spectrometer (Re-TOF). 62 species – among them 25 oxygenated molecules – were identified with the oxygenated species formed via oxidation of the hydrocarbon fragments formed in the decomposition of JP-10.

## 1. Introduction

Tricyclo[5.2.1.0<sup>2,6</sup>]decane (*exo*-tetrahydrodicyclopentadiene; *exo*-TCD) (Scheme 1) represents the principal constituent of the hydrocarbon jet fuel Jet Propellant-10 (JP-10; C<sub>10</sub>H<sub>16</sub>). JP-10 has attracted extensive attention from the experimental and theoretical communities to examine the features of the thermal decomposition and oxidation mechanisms, with attractive properties such as a high thermal stability, low freezing point, high-energy density, and high energy storage, [1–28]. Exploiting shock tubes, a comprehensive array of reactor types (flow tube, jet-stirred, tubular, batch), and most recently a high temperature chemical reactor, a detailed understanding of the *decomposition* of JP-10 is beginning to emerge. Here, the unimolecular decomposition of JP-10 surrogates lead to smaller hydrocarbon molecules and reactive intermediates, which *initiate* and *drive* the complex chemistry in the oxidation of JP-10 based jet fuel (Tables S1 and S2). Here, the initial decomposition chemistry, which is temporarily uncoupled from the oxidation stage, is often dubbed as ‘delivering the building blocks’ for the oxidation of JP-10.

Nevertheless, despite a decade of exploration, the basic, most fundamental processes controlling the *oxidation* of JP-10 have not been unraveled to date, predominantly because well-defined, experimentally and theoretically derived mechanistic information and identification of the nascent oxidation products are mainly lacking (Tables S3 and S4). Therefore, an innovative approach is proposed here to investigate the complete inventory of products and the underlying mechanisms of the oxidation JP-10 within a chemical micro reactor *in-situ* thus systematically advancing the current understanding of the fundamental, elementary processes, which *initiate* the complex chemistry in the oxidation of JP-10. Previously, Seiser et al. [21] conducted an experimental investigation on JP-10 counter-flow flames. Conditions of extinction and ignition were measured, and concentration profiles of key intermediates/products such as C1 to C8 species were recorded and modeled [29]. Hanson et al. [30] presented an experimental and kinetic modeling study on the ignition times and hydroxyl (OH) concentration in shock tube experiments for the JP-10 oxidation. A modeling work was performed, and sensitivity analysis indicated the possible role of the C2 chemistry in JP-10 decomposition. Colket and Spadaccini [31]

\* Corresponding author.

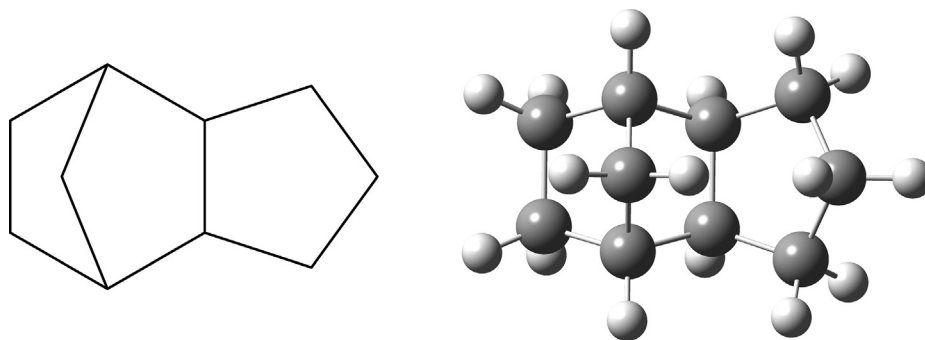
E-mail address: [ralfk@hawaii.edu](mailto:ralfk@hawaii.edu) (R.I. Kaiser).

<https://doi.org/10.1016/j.cplett.2020.137490>

Received 10 March 2020; Received in revised form 10 April 2020; Accepted 15 April 2020

Available online 18 April 2020

0009-2614/ © 2020 Elsevier B.V. All rights reserved.



Scheme 1. The molecular structure of JP-10 (exo-tetrahydrodicyclopentadiene).

presented shock tube studies on the ignition delay times of scramjet fuels including JP-10. This study exposed ignition-delay times decreasing in the sequence methane  $\rightarrow$  JP-10, heptane  $\rightarrow$  ethylene  $\rightarrow$  hydrogen. Mikolaitis et al. [9] measured the ignition of JP-10 at higher pressures (up to 25 atm) observing multiple concentration peaks of the methylidyne radical (CH) at the temperature over 1500 K. Wang et al. [26] probed JP-10 ignition measurements and concluded that in the high temperature range, the JP-10 concentration dependence of the ignition time suggests an enhanced ignition delay as the JP-10 concentration increases and/or the oxygen pressure drops. Most recently, Green et al. [27] carried out shock tube experiments probing ignition delay times of JP-10 combustion utilizing GC-MS to identify and quantify *stable* products. These studies revealed that JP-10 decomposes likely to ethylene (C<sub>2</sub>H<sub>4</sub>), propene (C<sub>3</sub>H<sub>6</sub>), cyclopentadiene (C<sub>5</sub>H<sub>6</sub>), and aromatics like benzene (C<sub>6</sub>H<sub>6</sub>) and toluene (C<sub>7</sub>H<sub>8</sub>). Apart from the experimental investigations, modeling and theoretical studies were also reported. Chenoweth et al. [5] carried out molecular dynamics simulations utilizing ReaxFF (reactive force field) investigations. In their simulation, JP-10 is initially oxidized on the methylene group leading eventually to a C-C bond scission followed by hydrogen abstraction. Further, Guo et al. [28] presented a ReaxFF molecular dynamics simulation concluding three reaction stages for the oxidation of JP-10. These are: i) the establishment of a pool of reactive radicals (H, O, OH, HO<sub>2</sub>), ii) the attack of these radicals to JP-10 and its decomposition fragments, and iii) follow up chain reactions of the initial degradation and oxidation intermediates.

Considering the lack of detailed chemical insights in the elementary processes of the oxidation of JP-10, the aforementioned compilation of previous studies suggests that the oxidation of JP-10 on the molecular level is far from being understood. Off-line and *ex-situ* analytical techniques (HPLC, GC-MS) provided clues on the formation of closed-shell products. However, reactive species cannot be sampled by these methods. The original information in the “molecular inventory” is likely to be misinterpreted by the utilization of off-line methods, leading to the loss of details on the reactions of intermediates, which are critical roles for reaction mechanisms. As a result, the necessary information for constructing reaction mechanisms derived from the off-line analysis is inferred only indirectly and qualitatively at best. Thus, a novel approach, which can probe both *stable* molecules and, in particular, thermally unstable species online and *in-situ* without chemically changing the initial pool of intermediates in the JP-10 oxidation, is required. The present investigation probes the oxidation of JP-10 (C<sub>10</sub>H<sub>16</sub>) in a high-temperature flow reactor at temperatures from 900 to 1031 K. The nascent oxidation intermediates/products are probed on line and *in-situ* in a supersonic molecular beam exploiting soft photoionization with single photon synchrotron vacuum ultraviolet (SVUV) light followed by a mass spectroscopic analysis of the ions in a reflectron time-of-flight mass spectrometer (Re-TOF-MS) [32–39]. By carrying out the molecular beam experiment, we elucidate data on all products, their branching ratios/mole fractions, as well as proposed reaction mechanisms involved in the oxidation of JP-10.

## 2. Experimental

The experiments were performed at the National Synchrotron Radiation Laboratory (NSRL) [32–37,39]. Briefly, the experimental setup consisted of three parts: a reaction chamber with a laminar flow reactor heated by a high-temperature furnace, a differentially pumped chamber, and a photoionization chamber housing a home-made RE-TOF-MS. JP-10 (C<sub>10</sub>H<sub>16</sub>) was kept in a stainless-steel bubbler at  $266 \pm 1$  K and was seeded in 760 Torr helium carrier gas (He, 99.999%). This gas mixture was then interspersed with krypton (Kr, 99.999%) as a calibrant gas and oxygen (O<sub>2</sub>, 99.999%). This mixture was fed into the reactor consisting of a 0.7 cm inner diameter alumina flow tube incorporating a 20.0 cm heated length in the high temperature furnace. The pressure inside the flow tube was regulated to 600 Torr. The flow of helium, krypton, and oxygen was controlled by mass flow controllers (1179A; MKS) at 780, 20 and 200 standard cubic centimeters per minute (SCCM), respectively, yielding an inlet mole fraction of JP-10 of 0.03%. The mole fractions of helium, krypton, and oxygen are determined as 77.98%, 2.00% and 19.99%, respectively, with errors of  $\pm 0.01\%$ . In this work, the equivalence ratio is determined to be 0.021 indicating extreme fuel-lean condition. The temperature range in the flow tube was monitored and controlled in the range from 900 K to 1031 K. At 1031 K, JP-10 is nearly completely decomposed, and, hence, no experiment was conducted at higher temperatures. The temperature profiles of the reactor are provided in Table S5. A quartz cone-shaped nozzle with a 100  $\mu$ m orifice was exploited to sample the species from the flow tube reactor within a molecular beam. The molecular beam passed into the photoionization chamber, where the neutral molecules are photoionized by tunable SVUV light from 8.00 eV to 11.50 eV with the stepsize of 0.05 eV. A set of additional mass spectra was collected at 14.80 eV to quantify water (H<sub>2</sub>O), carbon monoxide (CO), carbon dioxide (CO<sub>2</sub>), and methane (CH<sub>4</sub>). The photoionization efficiency curves (PIE), which report the intensity of an ion at a well-defined mass-to-charge ratio ( $m/z$ ) versus the photon energy, are exploited to unambiguously identifying oxidation intermediates [40]. In this work, the PIE curves were extracted in the energy range from 8.00 eV to 11.50 eV, which covers the ionization energies (IE) of critical species generated in the oxidation process except water (IE = 12.62 eV), carbon monoxide (IE = 14.0 eV), carbon dioxide (IE = 13.78 eV), and methane (IE = 12.61 eV). Several species may contribute to a PIE of a well-defined  $m/z$ . Therefore, the PIEs have to be fit with a linear combination of calibration PIE curves of multiple structural isomers (reference curves), which can contribute to the specific  $m/z$ . In this work, the PIE reference curves are taken from an online database (Table S6) [41].

## 3. Experimental results

Fig. 1 exhibited typical mass spectra collected during the oxidation of JP-10 (C<sub>10</sub>H<sub>16</sub>,  $m/z = 136$ ) at distinct temperatures. The photon energy in Fig. 1 is chosen at 10 eV due to the fact that JP-10 can be

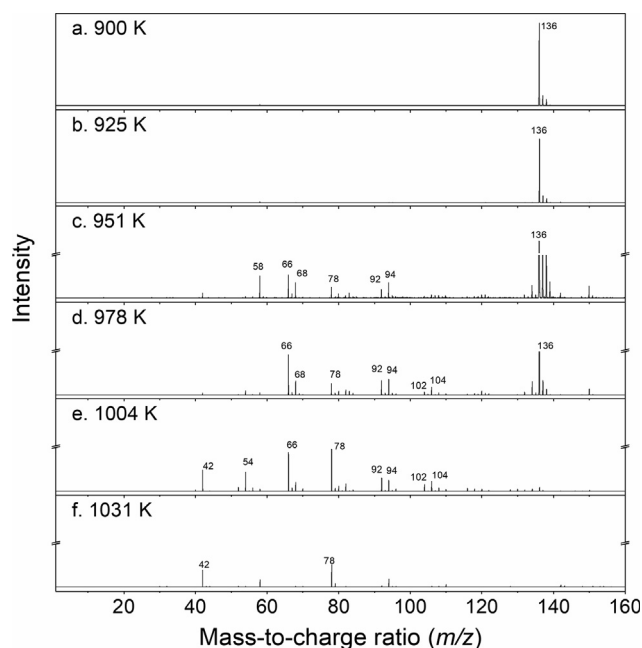


**Fig. 1.** Mass spectra of the products obtained from the oxidation of JP-10 recorded in NSRL at a photon energy of 10.0 eV at different temperatures from 900 K to 1031 K.

photodissociated when the energy is higher than 10 eV. The mass spectrometric data provide explicit evidence of ion counts of the ionized neutral products from at least  $m/z = 42$  to  $m/z = 154$  along with the parent ions of the ionized JP-10 precursor at  $m/z = 136$ . The corresponding photoionization efficiency (PIE) curves along with the best fits are visualized in Figs. 2 and S1 at a reactor temperature of 1004 K. Generally, the black lines present the PIE curve as extracted from the experimental data with the shaded area exhibiting the experimental uncertainties. The red lines are the overall best fit to the PIE curves. If the PIE curves have multiple contributors, other colored lines are referred to individual components as defined in the panels. The detected mass-to-charge ratios, as well as the chemical formulae and chemical structures of the assigned products are compiled in Tables S7 and S8.

In this work, the intensity of the parent ion of JP-10 ( $m/z = 136$ ) decreases with the temperature increasing from 100% (900 K) via 98.9% (925 K), 85.6% (951 K), 59.0% (978 K), 1.4% (1004 K), to < 0.1% at 1031 K (Fig. 3). Previous pyrolysis experiment of JP-10 without oxygen suggests that JP-10 was decomposed from 100% (927 K) to almost complete decomposition at 1083 K [42]. Comparing the oxidation and pyrolysis results, JP-10 starts and fully completes the decomposition at lower temperatures in the presence of oxygen. Further, the decomposition(oxidation) range is much narrower in the presence of oxygen indicating a higher reactivity toward decomposition (oxidation).

The mass spectrometric data reveal evidence of ion counts from  $m/z = 16$  to  $m/z = 154$ . Two molecules heavier than JP-10 were observed in the experiment with molecular weights of 142 amu ( $C_{11}H_{12}$ ) and 154 amu ( $C_{12}H_{10}$ ). As compiled in Tables S7 and S8, as the temperature increases, the number of oxidation products first rises from 17 at 925 K to 27 (951 K), 48 (978 K), 61 (1004 K) and then drops to 47 (1031 K). At 978 K, the highest number of products were observed with most of their concentrations reaching the maxima. Considering the significant number of conceivable isomers, some unidentified intermediates/products generated might exist as evident from discrepancies presented in the fits of the PIE curves especially for higher molecular weight products where PIE reference curves of all possible isomers are not available.

A total of 62 products at distinct temperatures including hydrocarbons and oxygen-bearing molecules are observed and identified. The hydrocarbons can be arranged into eleven groups. i) alkanes [methane ( $CH_4$ )], ii) alkenes [ethylene ( $C_2H_4$ ), propene ( $C_3H_6$ ), 1-butene ( $C_4H_8$ ), *cis*-2-butene ( $C_4H_8$ ), 1-hexene ( $C_6H_{12}$ ), *trans*-2-hexene ( $C_6H_{12}$ )], iii) dienes [1,3-butadiene ( $C_4H_6$ ), 1,4-pentadiene ( $C_5H_8$ ), 2,4-hexadiene ( $C_6H_{10}$ )], iv) C3-C4 cumulenes [allene ( $C_3H_4$ ), 1,2,3-butatriene ( $C_4H_4$ )], v) alkynes (acetylene ( $C_2H_2$ ), methylacetylene ( $C_3H_4$ )), vi) enyne [vinylacetylene ( $C_4H_4$ )], vii) cyclodienes [cyclopentadiene ( $C_5H_6$ ), 1,3-cyclohexadiene ( $C_6H_8$ )], viii) cycloalkene [cyclohexene ( $C_6H_{10}$ )], ix) cycloalkane [cyclohexane ( $C_6H_{12}$ )], x) aromatics [benzene ( $C_6H_6$ ), toluene ( $C_7H_8$ ), phenylacetylene ( $C_8H_6$ ), styrene ( $C_8H_8$ ), *o*-xylene ( $C_8H_{10}$ ), indene ( $C_9H_8$ ), indane ( $C_9H_{10}$ ), 1,3,5-trimethylbenzene ( $C_9H_{12}$ ), naphthalene ( $C_{10}H_8$ ), 1,2-dihydronaphthalene ( $C_{10}H_{10}$ ), 2-methylpropenylbenzene ( $C_{10}H_{12}$ ), 1-methylnaphthalene ( $C_{11}H_{10}$ ), biphenyl ( $C_{12}H_{10}$ )], and xi) 'special' products which could not be grouped to the aforementioned series [fulvene ( $C_6H_6$ ), fulvenallene ( $C_7H_6$ ), 5-methylene-1,3-cyclohexadiene ( $C_7H_8$ ), 1,3,5-cyclooctatriene ( $C_8H_{10}$ ), and 1,4,5,8-tetrahydronaphthalene ( $C_{10}H_{12}$ )]. It is critical to highlight that in these experiments, no radicals were detected. The reactor pressure of 600 Torr and the residence time of  $120 \pm 20$  ms leads either to the decomposition of the radicals or the successive reaction (oxidation). Besides, some of the products listed above [5-ethenylidene-1,3-cyclopentadiene ( $C_7H_8$ , IE = 7.9 eV) [43], 1,3,5-cyclooctatriene ( $C_8H_{10}$ , IE = 7.9 eV) [44], 2-methylpropenylbenzene ( $C_{10}H_{12}$ , IE = 7.78 eV) [45], and 1-methylnaphthalene ( $C_{11}H_{10}$ , IE = 7.9 eV) [46]] have photoionization energies below 8.0 eV, lower than the experiment energy range. Thus, these species were identified based on the PIE fitting rather than confirming their ionization energy. For the oxidation products, there are overall 25 of them observed. Based on their functional groups, these can be arranged into nine groups: i) alcohols [methanol ( $CH_4O$ ), ethanol ( $C_2H_6O$ ), benzyl alcohol ( $C_7H_8O$ ), 1,2-benzenediol ( $C_6H_6O_2$ )], ii) enols [ethenol ( $C_2H_4O$ )], iii) enal [2-butenal ( $C_4H_6O$ )], iv) aldehydes [formaldehyde ( $CH_2O$ ), acetaldehyde ( $C_2H_4O$ ), propanal ( $C_3H_6O$ ), benzaldehyde ( $C_7H_6O$ ), methylbenzaldehydes ( $C_8H_8O$ )], v) ketene [ketene ( $C_2H_2O$ )], vi) ketones [acetone ( $C_3H_6O$ ), 2,4-cyclopentadiene-1-one ( $C_5H_4O$ ), 2-cyclopentan-1-one ( $C_5H_6O$ ), 1,4-cyclohex-2-enedione ( $C_6H_6O_2$ ), *p*-benzoquinone ( $C_6H_4O_2$ )], vii) hydroxybenzene [phenol ( $C_6H_6O$ ), cresols ( $C_7H_8O$ ), and dimethylphenols ( $C_8H_{10}O$ )], viii) cyclic ethers furan ( $C_4H_4O$ ), 2,3-dihydrofuran ( $C_4H_6O$ )], and ix) terminal (end) products of the oxidation [water ( $H_2O$ ), carbon monoxide (CO), carbon dioxide ( $CO_2$ )]. It should be noticed that due to the lack of calibration PIEs and/or photoionization cross sections of the related species, especially for those with higher molecular weights, some isomers are merged into classes: cresols ( $C_7H_8O$ ), methylbenzaldehydes ( $C_8H_8O$ ), and dimethylphenols ( $C_8H_{10}O$ ).

## 4. Discussion

A quantitative analysis of the detected products is performed with branching ratios in Table 1 and Fig. S2. The digital data of the mole fractions are also provided in Table S9. The analysis of the temperature dependence of the PIE curves reveals interesting trends, as discussed in the following two sections, hydrocarbons and oxygenated species.

### 4.1. Hydrocarbon products

First, as evident from Table 1, ethylene ( $C_2H_4$ ) represents the major C2 hydrocarbon product of JP-10; its overall product fraction increases from 1.8% at 978 K to 2.1% at 1004 K and then decreases to 0.4% at 1031 K. For acetylene ( $C_2H_2$ ), the branching ratio is nearly invariant on the temperature from 1004 K to 1031 K reaching levels of close to 0.4%. The overall branching ratio of all C2 hydrocarbons first increases from 2.2% at 978 K to 2.5% at 1004 K and then drops to 0.7% due to the formation of additional products as discussed below.

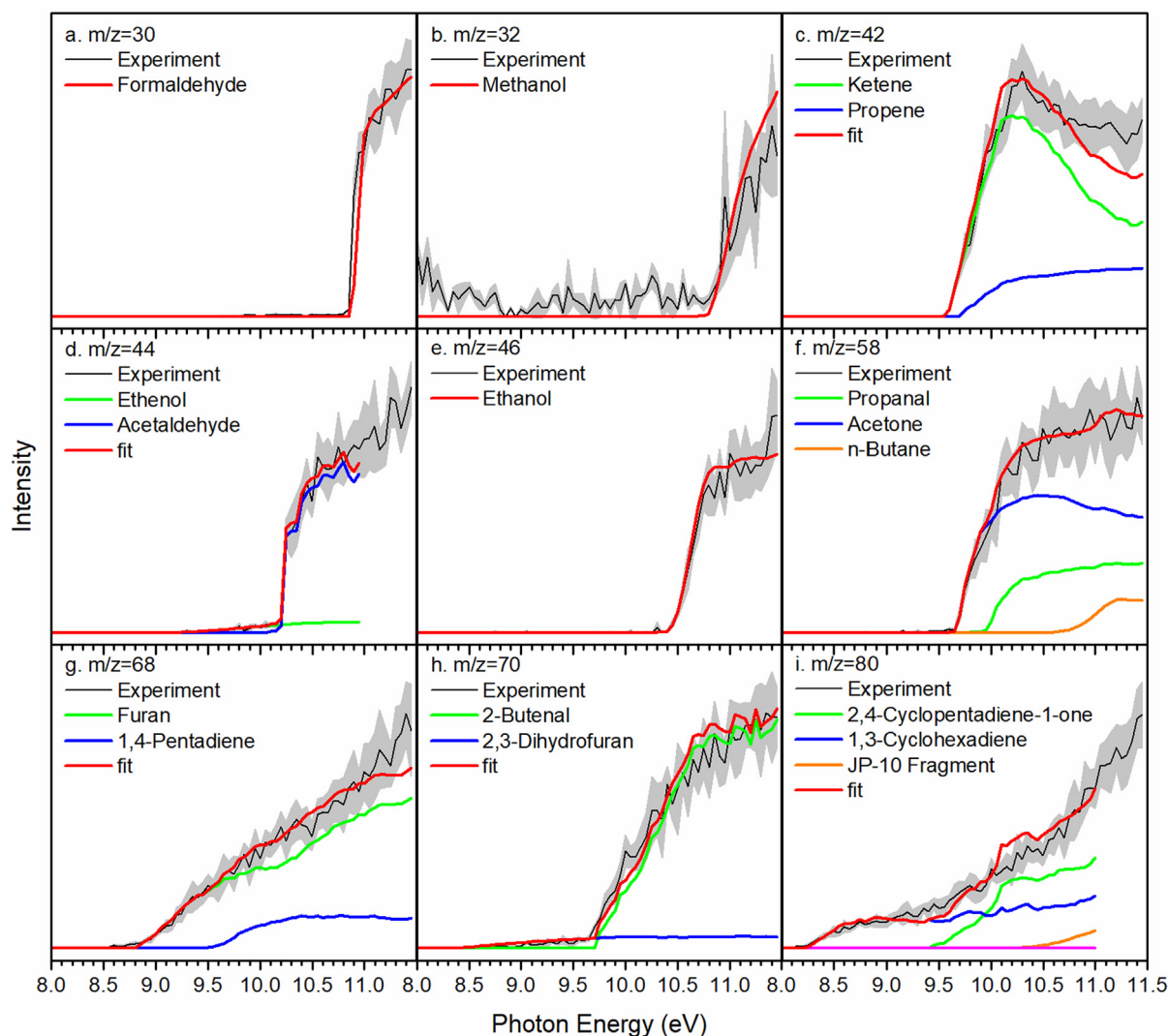


**Fig. 2.1.** Experimental photoionization efficiency curves (PIE, black lines) for oxygenated species recorded from the oxidation of JP-10 (NSRL) at 1004 K along with the experimental errors (gray area) and the reference PIE curves (blue, green and red lines). In the case of multiple contributions to one PIE curve, the red line resembles the overall fit.

Second, three C3 species were observed: allene ( $C_3H_4$ ), methylacetylene ( $C_3H_4$ ), and propene ( $C_3H_6$ ). Among these products, propene dominates (0.3% at 1004 K). As the temperature increases to 1031 K, it is nearly completely decomposed to levels lower than 0.1%. The total branching ratios of allene and methylacetylene increases from 0.1% (978 K) to 0.2% (1004 K). In the temperature range from 978 K to 1004 K, the branching ratios of allene and methylacetylene increase, while the branching ratio of propene remains around 0.3% indicating that both  $C_3H_4$  isomers might be products from the decomposition of propene.

Third, five C4 hydrocarbon species were observed and quantified: 1,2,3-butatriene ( $C_4H_4$ ), vinylacetylene ( $C_4H_4$ ), 1,3-butadiene ( $C_4H_6$ ), 1-butene ( $C_4H_8$ ), and 2-butene ( $C_4H_8$ ). Their production yields are quite low except for 1,3-butadiene and 1-butene. Both species are formed at 978 K with branching ratios of 0.5% and 0.8%; these numbers increase both to 1.0% with rising temperature to 1004 K. All branching ratios of the remaining C4 species are below 0.5%.

Fourth, cyclopentadiene ( $C_5H_6$ ) represents a key C5 species in the JP-10 oxidation [1,11,16,47,48]. It is detected at 925 K and reaches to the maximum branching ratio value of 6% at 978 K. This low appearance temperature illustrates that cyclopentadiene represents likely an initial and major product in the JP-10 decomposition; this suggestion agrees with the conclusion that cyclopentadiene was detected as one of

the key products in previous JP-10 pyrolysis studies [42]. A second C5 species detected in this work is 1,4-pentadiene ( $C_5H_8$ ). The branching ratio of 1,4-pentadiene decreases from 1.7% at 951 K to 0.01% at 1031 K, possibly because 1,4-pentadiene represents one of the key reaction intermediates in the JP-10 decomposition route.

Fifth, fulvene ( $C_6H_6$ ), benzene ( $C_6H_6$ ), 1,3-cyclohexadiene ( $C_6H_8$ ), cyclohexene ( $C_6H_{10}$ ), 2,4-hexadiene ( $C_6H_{10}$ ), 1-hexene ( $C_6H_{12}$ ), *trans*-2-hexene ( $C_6H_{12}$ ), and cyclohexane ( $C_6H_{12}$ ) constitute the C6 hydrocarbon series in the JP-10 oxidation. Fulvene and cyclohexene likely define initial products formed at 925 K illustrating - based on the temperature-dependent branching ratios - that they represent intermediates leading to the formation of smaller species. With increasing temperature, the branching ratio of fulvene rises from 0.6% at 925 K to 1.7% at 951 K, drops to 0.03% at 1004 K; at 1031 K, it is fully decomposed. Meanwhile, the branching ratios of cyclohexene starts from 12% at 925 K to its maximum value of 46% at 978 K; hereafter it decreases to its complete decomposition at 1031 K via a ratio of 32% at 1004 K. As the temperature rises, the concentration of fulvene decreases at the expense of benzene suggesting that one of the loss pathways of fulvene is the isomerization process to benzene [49]. Some  $C_6H_{12}$  isomers appear at 951 K, but their yields quickly drop to zero at 1031 K indicating that they might be initial decomposition intermediates.

Sixth, hydrocarbons larger than C7 represent minor, but still

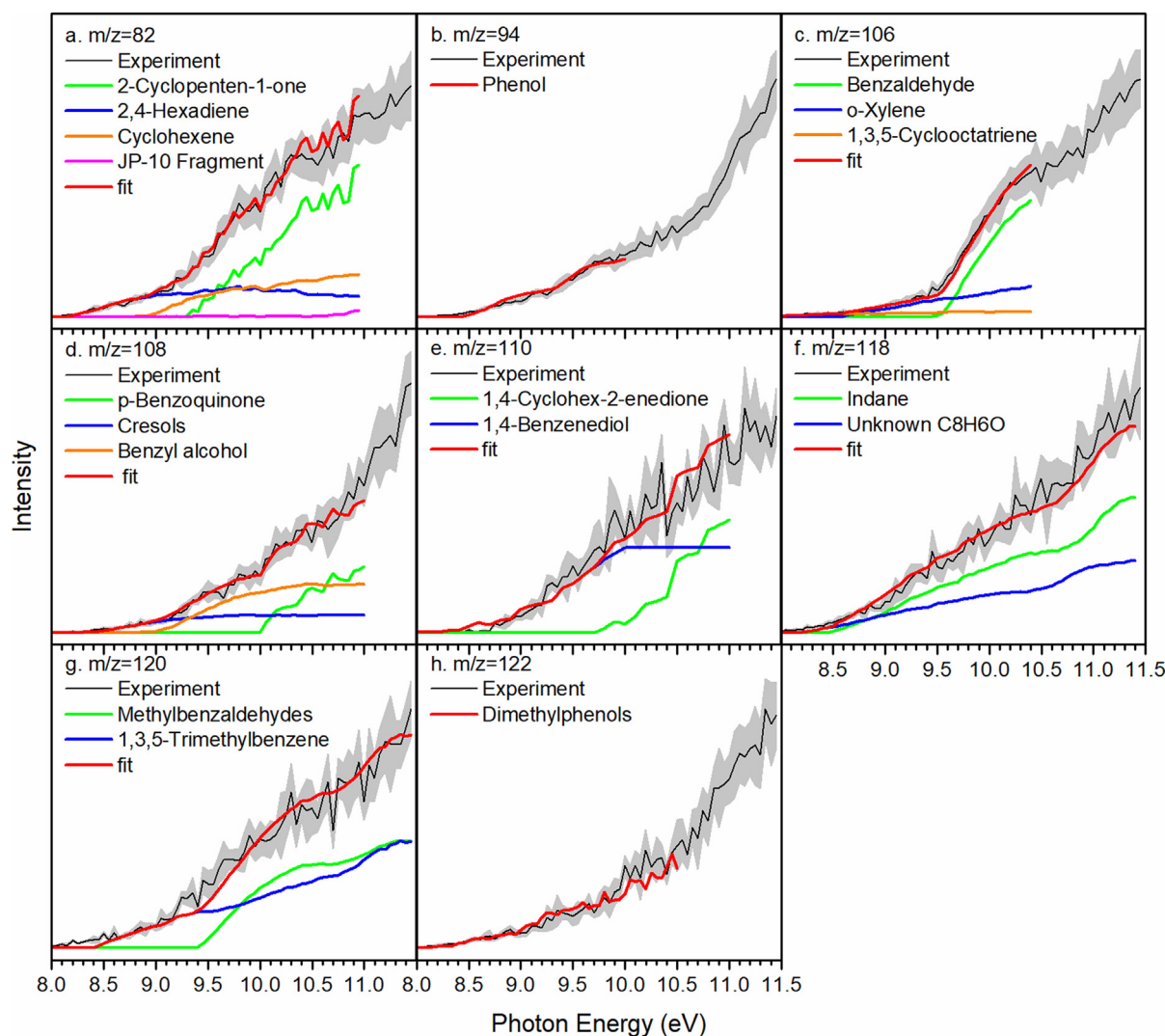


**Fig. 2.2.** Experimental photoionization efficiency curves (PIE, black lines) for oxygenated species recorded from the oxidation of JP-10 at 1004 K along with the experimental errors (gray area) and the reference PIE curves (blue, green and red lines). In the case of multiple contributions to one PIE curve, the red line resembles the overall fit.

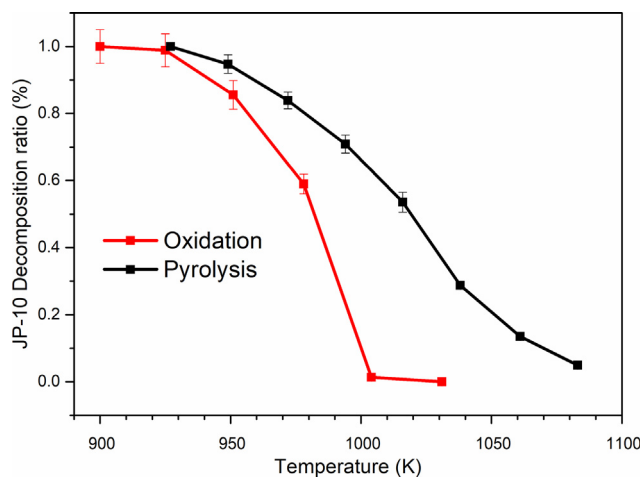


**Fig. 3.** JP-10 decomposition ratios in the oxidation (current work, red) and previous pyrolysis experiments (black) [42].

mechanistically important products. Three C7 species are: fulvenallene ( $C_7H_6$ ), 5-methylene-1,3-cyclohexadiene ( $C_7H_8$ ), and toluene ( $C_7H_8$ ). Besides, four C8 products, two C9 products and four C10 products were detected, too (Table S7, Figs. 2 and S1). 5-Methylene-1,3-cyclohexadiene ( $C_7H_8$ ) was observed at a low temperature of 951 K indicating that this species represents one of the primary intermediates of JP-10 decomposition; this conclusion also holds for *o*-xylene ( $C_8H_{10}$ ) and 1,3,5-cyclooctatriene ( $C_8H_{10}$ ). The C7 and C8 species are produced only at higher temperatures suggesting that those molecules represent likely higher-order products. Indane and indene both appear at high temperatures with the branching ratios below 0.3%. The branching ratios of naphthalene ( $C_{10}H_8$ ), 1,2-dihydronaphthalene ( $C_{10}H_{10}$ ), 1,4,5,8-tetrahydronaphthalene ( $C_{10}H_{12}$ ) and 2-methylpropenylbenzene ( $C_{10}H_{12}$ ) are very small ( $< 0.7\%$ ) and are detected at relatively high temperatures of 1004 K suggesting that these molecules could be higher order products likely formed via recombination/reaction of smaller species, possibly radicals. Finally, with longer residence times, larger PAHs can be synthesized. Two PAHs with molecular weights higher than JP-10 were observed: 1-methylnaphthalene ( $C_{11}H_{10}$ ) and biphenyl ( $C_{12}H_{10}$ ). These products are generated only higher temperatures of 1004 K. It is proposed that these PAHs form as higher order reaction products.

**Table 1**  
Branching ratios (%) of the products in the oxidation of JP-10 at 600 Torr in the chemical reactor at 925, 951, 978, 1004 and 1031 K. The numbers in each bracket present the lower and upper uncertainties, respectively. Some of the error bars are quite large due to the relatively high uncertainties of photoionization cross sections (20% for experimentally measured photoionization cross sections, and a factor of 2 for the estimated).

Molecules	Formula	Measured IE (eV)	Temperature				
			925 K	951 K	978 K	1004 K	1031 K
Methane	CH <sub>4</sub>	-	0 (0, 0)	0 (0, 0)	0 (0, 0)	0.203 (-0.03, 0.03)	0.190 (-0.028, 0.028)
Water	H <sub>2</sub> O	-	63.172 (-9.476, 9.476)	33.96 (-5.094, 5.094)	7.1 (-1.065, 1.065)	14.419 (-2.163, 2.163)	29.203 (-4.381, 4.381)
Acetylene	C <sub>2</sub> H <sub>2</sub>	11.40 ± 0.05	0 (0, 0)	0 (0, 0)	0 (0, 0)	0.435 (-0.14, 0.14)	0.350 (-0.171, 0.171)
Carbon monoxide	CO	-	8.579 (-1.287, 1.287)	6.772 (-1.016, 1.016)	10.344 (-1.552, 1.552)	27.454 (-4.118, 4.118)	43.599 (-6.54, 6.54)
Ethylene	C <sub>2</sub> H <sub>4</sub>	10.50 ± 0.05	0 (0, 0)	0 (0, 0)	1.765 (-0.696, 0.696)	2.105 (-0.731, 0.731)	0.398 (-0.164, 0.164)
Formaldehyde	CH <sub>2</sub> O	10.90 ± 0.05	0.415 (-0.276, 0.483)	0.527 (-0.367, 0.63)	0.487 (-0.4, 0.643)	0.744 (-0.514, 0.886)	0.197 (-0.147, 0.245)
Methanol	CH <sub>3</sub> O	10.85 ± 0.05	0 (0, 0)	0 (0, 0)	0.013 (-0.009, 0.009)	0.026 (-0.013, 0.013)	0.02 (-0.005, 0.005)
Allene	C <sub>3</sub> H <sub>4</sub>	9.70 ± 0.05	0 (0, 0)	0 (0, 0)	0.050 (-0.01, 0.01)	0.118 (-0.032, 0.032)	0.017 (-0.009, 0.009)
Methylacetylene	C <sub>3</sub> H <sub>4</sub>	10.35 ± 0.05	0 (0, 0)	0 (0, 0)	0.041 (-0.014, 0.014)	0.110 (-0.033, 0.033)	0.015 (-0.005, 0.005)
Ketene	C <sub>2</sub> H <sub>2</sub> O	9.60 ± 0.05	0 (0, 0)	0 (0, 0)	0.184 (-0.212, 0.212)	0.623 (-0.361, 0.361)	0.031 (-0.036, 0.036)
Propene	C <sub>3</sub> H <sub>6</sub>	9.70 ± 0.05	0.436 (-0.241, 0.241)	0.323 (-0.371, 0.371)	0.259 (-0.294, 0.294)	0.31 (-0.256, 0.256)	0.04 (-0.046, 0.046)
Ethanol	C <sub>2</sub> H <sub>5</sub> O	9.30 ± 0.05	0 (0, 0)	0 (0, 0)	0.015 (-0.018, 0.018)	0.035 (-0.005, 0.005)	0.008 (-0.005, 0.005)
Acetaldehyde	C <sub>2</sub> H <sub>4</sub> O	10.20 ± 0.05	0 (0, 0)	0 (0, 0)	0.115 (-0.019, 0.019)	0.450 (-0.083, 0.083)	0.034 (-0.011, 0.011)
Carbon dioxide	CO <sub>2</sub>	-	6.295 (-0.944, 0.944)	9.519 (-1.428, 1.428)	2.019 (-0.303, 0.303)	4.709 (-0.706, 0.706)	24.24 (-3.636, 3.636)
Ethanol	C <sub>2</sub> H <sub>6</sub> O	10.45 ± 0.05	0 (0, 0)	0 (0, 0)	0.823 (-0.168, 0.168)	0.282 (-0.111, 0.111)	0.345 (-0.131, 0.131)
1,2,3-butatriene	C <sub>4</sub> H <sub>4</sub>	9.25 ± 0.05	0 (0, 0)	0 (0, 0)	0.012 (-0.018, 0.025)	0.004 (-0.006, 0.008)	0 (0, 0)
Vinylacetylene	C <sub>4</sub> H <sub>4</sub>	9.60 ± 0.05	0 (0, 0)	0 (0, 0)	0.007 (-0.006, 0.006)	0.073 (-0.017, 0.017)	0.010 (-0.006, 0.006)
1,3-Butadiene	C <sub>4</sub> H <sub>6</sub>	9.05 ± 0.05	0 (0, 0)	0 (0, 0)	0.468 (-0.126, 0.126)	0.984 (-0.213, 0.213)	0.011 (-0.006, 0.006)
1-Butene	C <sub>4</sub> H <sub>8</sub>	9.60 ± 0.05	0 (0, 0)	0.167 (-0.147, 0.147)	0.807 (-0.491, 0.491)	0.999 (-0.339, 0.339)	0.049 (-0.011, 0.011)
cis-2-Butene	C <sub>4</sub> H <sub>8</sub>	9.10 ± 0.05	0 (0, 0)	0.059 (-0.068, 0.068)	0.067 (-0.034, 0.034)	0.266 (-0.144, 0.144)	0.009 (-0.01, 0.01)
Propanal	C <sub>3</sub> H <sub>6</sub> O	9.95 ± 0.05	0 (0, 0)	0 (0, 0)	0.451 (-0.11, 0.11)	0.241 (-0.07, 0.07)	0.177 (-0.03, 0.03)
Acetone	C <sub>3</sub> H <sub>6</sub> O	9.70 ± 0.05	0 (0, 0)	0 (0, 0)	0.594 (-0.202, 0.202)	0.284 (-0.096, 0.096)	0.267 (-0.073, 0.073)
Cyclopentadiene	C <sub>5</sub> H <sub>6</sub>	8.55 ± 0.05	1.397 (-0.516, 0.516)	4.316 (-1.325, 1.325)	5.709 (-1.321, 1.321)	2.779 (-1.037, 1.037)	0.010 (-0.009, 0.009)
Furan	C <sub>4</sub> H <sub>4</sub> O	8.85 ± 0.05	0.918 (-0.345, 0.345)	2.775 (-0.985, 0.985)	2.441 (-1.012, 1.012)	0.692 (-0.279, 0.279)	0.027 (-0.022, 0.022)
1,4-Pentadiene	C <sub>5</sub> H <sub>8</sub>	9.55 ± 0.05	1.849 (-0.412, 0.412)	1.698 (-0.316, 0.316)	1.836 (-0.285, 0.285)	0.367 (-0.112, 0.112)	0.010 (-0.002, 0.002)
2-Butenal	C <sub>4</sub> H <sub>6</sub> O	9.70 ± 0.05	0 (0, 0)	0 (0, 0)	0.189 (-0.039, 0.039)	0.277 (-0.07, 0.07)	0.02 (-0.007, 0.007)
3,3-Dihydrofuran	C <sub>4</sub> H <sub>6</sub> O	8.35 ± 0.05	0 (0, 0)	0 (0, 0)	0.039 (-0.022, 0.022)	0.033 (-0.011, 0.011)	0.001 (-0.002, 0.002)
Fulvene	C <sub>6</sub> H <sub>6</sub>	8.30 ± 0.05	0.593 (-0.195, 0.195)	1.725 (-1.181, 1.181)	1.742 (-0.292, 0.292)	0.275 (-0.059, 0.059)	0 (0, 0)
Benzene	C <sub>6</sub> H <sub>6</sub>	9.20 ± 0.05	0 (0, 0)	0.115 (-0.132, 0.132)	0.168 (-0.093, 0.093)	1.252 (-0.229, 0.229)	0.335 (-0.078, 0.078)
1,3-Cyclohexadiene	C <sub>6</sub> H <sub>8</sub>	8.25 ± 0.05	0 (0, 0)	0.141 (-0.095, 0.095)	0.362 (-0.103, 0.103)	0.213 (-0.048, 0.048)	0.002 (-0.002, 0.002)
2,4-Cyclopentadiene-1-one	C <sub>5</sub> H <sub>4</sub> O	9.40 ± 0.05	0.025 (-0.038, 0.051)	0.062 (-0.049, 0.079)	0.138 (-0.071, 0.14)	0.109 (-0.076, 0.13)	0.001 (-0.001, 0.002)
Cyclohexene	C <sub>6</sub> H <sub>10</sub>	8.95 ± 0.05	11.96 (-13.754, 13.754)	21.604 (-19.699, 19.699)	45.501 (-7.208, 7.208)	31.573 (-5.537, 5.537)	0 (0, 0)
2-Cyclopenten-1-one	C <sub>5</sub> H <sub>6</sub> O	9.30 ± 0.05	0.177 (-0.265, 0.354)	0.479 (-0.377, 0.616)	0.948 (-0.534, 1.008)	0.861 (-0.521, 0.952)	0.017 (-0.01, 0.019)
2,4-Hexadiene	C <sub>6</sub> H <sub>12</sub>	8.20 ± 0.05	0 (0, 0)	0 (0, 0)	0.68 (-0.102, 0.102)	0.506 (-0.076, 0.076)	0.017 (-0.003, 0.003)
1-Hexene	C <sub>6</sub> H <sub>12</sub>	9.45 ± 0.05	0 (0, 0)	0.117 (-0.022, 0.022)	0.007 (-0.008, 0.008)	0.007 (-0.008, 0.008)	0 (0, 0)
trans-2-Hexene	C <sub>6</sub> H <sub>12</sub>	8.95 ± 0.05	0 (0, 0)	0.428 (-0.245, 0.245)	0 (0, 0)	0 (0, 0)	0 (0, 0)
Cyclohexane	C <sub>6</sub> H <sub>12</sub>	9.90 ± 0.05	0 (0, 0)	0.148 (-0.094, 0.168)	0.059 (-0.089, 0.118)	0.008 (-0.011, 0.015)	0.001 (-0.001, 0.001)
Fulvenallene	C <sub>7</sub> H <sub>6</sub>	8.30 ± 0.05	0 (0, 0)	0 (0, 0)	0 (0, 0)	0.00005 (-0.00003, 0.00005)	0 (0, 0)
5-Methylene-1,3-cyclohexadiene	C <sub>7</sub> H <sub>8</sub>	-	2.55 (-0.799, 0.799)	8.338 (-3.542, 3.542)	6.643 (-2.065, 2.065)	1.931 (-0.495, 0.495)	0 (0, 0)
Toluene	C <sub>7</sub> H <sub>8</sub>	8.80 ± 0.05	0.389 (-0.136, 0.136)	0.379 (-0.169, 0.169)	0.871 (-0.208, 0.208)	0.456 (-0.1, 0.1)	0.011 (-0.002, 0.002)
Phenol	C <sub>6</sub> H <sub>6</sub> O	8.95 ± 0.05	0.63 (-0.282, 0.282)	1.754 (-0.306, 0.306)	1.808 (-0.356, 0.356)	0.437 (-0.102, 0.102)	0.128 (-0.039, 0.039)
Phenylacetylene	C <sub>8</sub> H <sub>6</sub>	8.80 ± 0.05	0 (0, 0)	0 (0, 0)	0 (0, 0)	0.002 (-0.001, 0.001)	0 (0, 0)
Styrene	C <sub>8</sub> H <sub>8</sub>	8.45 ± 0.05	0 (0, 0)	0 (0, 0)	0.240 (-0.04, 0.04)	0.332 (-0.122, 0.122)	0.010 (-0.006, 0.006)
1,3,5-Cyclooctatriene	C <sub>8</sub> H <sub>10</sub>	9.55 ± 0.05	0.158 (-0.238, 0.317)	1.930 (-2.328, 3.292)	1.337 (-0.947, 1.616)	0.161 (-0.146, 0.226)	0 (0, 0)
o-Xylene	C <sub>8</sub> H <sub>10</sub>	9.50 ± 0.05	0.456 (-0.525, 0.525)	1.119 (-0.339, 0.339)	1.476 (-0.281, 0.281)	0.259 (-0.04, 0.04)	0.013 (-0.006, 0.006)
Benzaldehyde	C <sub>7</sub> H <sub>6</sub> O	10.00 ± 0.05	0 (0, 0)	0 (0, 0)	0 (0, 0)	0.178 (-0.096, 0.185)	0.005 (-0.007, 0.01)
p-Benzoquinone	C <sub>6</sub> H <sub>4</sub> O <sub>2</sub>	8.30 ± 0.05	0 (0, 0)	0.226 (-0.339, 0.452)	0.359 (-0.273, 0.453)	0.146 (-0.165, 0.238)	0 (0, 0)
Cresols	C <sub>7</sub> H <sub>8</sub> O	8.30 ± 0.05	0 (0, 0)	0 (0, 0)	0.285 (-0.153, 0.153)	0.169 (-0.123, 0.123)	0 (0, 0)
Benzyl alcohol	C <sub>7</sub> H <sub>8</sub> O	8.85 ± 0.05	0 (0, 0)	0 (0, 0)	0 (0, 0)	0.028 (-0.042, 0.056)	0.01 (-0.01, 0.015)
1,4-Cyclohex-2-enedione	C <sub>6</sub> H <sub>4</sub> O <sub>2</sub>	9.75 ± 0.05	0 (0, 0)	0 (0, 0)	0.051 (-0.051, 0.077)	0.023 (-0.035, 0.047)	0 (0, 0)
1,4-Benzenedione	C <sub>6</sub> H <sub>4</sub> O <sub>2</sub>	-	0 (0, 0)	1.189 (-0.46, 0.46)	0.33 (-0.07, 0.07)	0.13 (-0.046, 0.046)	0.091 (-0.031, 0.031)

(continued on next page)

Table 1 (continued)

Molecules	Formula	Measured IE (eV)	Temperature				
			925 K	951 K	978 K	1004 K	1031 K
Indene	C <sub>9</sub> H <sub>8</sub>	8.15 ± 0.05	0 (0, 0)	0 (0, 0)	0 (0, 0)	0 (0, 0)	0 (0, 0)
Indane	C <sub>9</sub> H <sub>10</sub>	8.55 ± 0.05	0 (0, 0)	0 (0, 0)	0.194 (-0.107, 0.203)	0.076 (-0.018, 0.018)	0.002 (-0.003, 0.004)
Methylbenzaldehydes	C <sub>8</sub> H <sub>8</sub> O	9.30 ± 0.05	0 (0, 0)	0 (0, 0)	0.325 (-0.054, 0.054)	0.099 (-0.028, 0.028)	0.004 (-0.004, 0.004)
1,3,5-Trimethylbenzene	C <sub>9</sub> H <sub>12</sub>	8.40 ± 0.05	0 (0, 0)	0 (0, 0)	0.569 (-0.295, 0.579)	0.081 (-0.042, 0.082)	0.005 (-0.008, 0.011)
Dimethylphenols	C <sub>8</sub> H <sub>10</sub> O	8.10 ± 0.05	0 (0, 0)	0.130 (-0.123, 0.188)	0.073 (-0.04, 0.077)	0.028 (-0.016, 0.03)	0.006 (-0.006, 0.008)
Naphthalene	C <sub>10</sub> H <sub>8</sub>	8.15 ± 0.05	0 (0, 0)	0 (0, 0)	0 (0, 0)	0.785 (-0.55, 0.943)	0.036 (-0.025, 0.043)
1,2-Dihydronaphthalene	C <sub>10</sub> H <sub>10</sub>	8.00 ± 0.05	0 (0, 0)	0 (0, 0)	0 (0, 0)	0.041 (-0.021, 0.042)	0 (0, 0.001)
1,4,5,8-Tetrahydronaphthalene	C <sub>10</sub> H <sub>12</sub>	8.00 ± 0.05	0 (0, 0)	0 (0, 0)	0 (0, 0)	0.552 (-0.36, 0.636)	0.010 (-0.015, 0.02)
2-Methylpropenylbenzene	C <sub>10</sub> H <sub>12</sub>	8.45 ± 0.05	0 (0, 0)	0 (0, 0)	0 (0, 0)	0.055 (-0.017, 0.017)	0 (0, 0)
1-Methylnaphthalene	C <sub>11</sub> H <sub>10</sub>	-	0 (0, 0)	0 (0, 0)	0 (0, 0)	0.024 (-0.013, 0.024)	0.018 (-0.011, 0.02)
Biphenyl	C <sub>12</sub> H <sub>10</sub>	8.15 ± 0.05	0 (0, 0)	0 (0, 0)	0 (0, 0)	0.008 (-0.006, 0.01)	0 (0, 0)

## 4.2. Oxygen bearing products

First, there four C1 oxygenated species including carbon monoxide (CO), carbon dioxide (CO<sub>2</sub>), formaldehyde (CH<sub>2</sub>O), and methanol (CH<sub>3</sub>OH) were detected. Formaldehyde appears at the temperature of 925 K, indicating it represents an initial product. The decomposition of formaldehyde could lead to the formation of carbon monoxide. Further oxidation of carbon monoxide will yield carbon dioxide. Carbon monoxide and carbon dioxide are the most important products in the oxidation process. They both appear at the temperature of 925 K and reach branching ratios of 44% and 24%, respectively, at 1031 K; at this temperature, most of the remaining species are consumed. Methanol represents a minor fraction and appears at higher temperatures (978 K) compared to the remaining C1 oxygenated species. Apart from carbon monoxide and carbon dioxide, water (H<sub>2</sub>O) is one of the final products and largely produced at low temperature of 925 K with branching ratios up to 56%. With the temperature increasing and additional C1 species being produced, the branching ratio reduces to 29% at 1031 K.

Second, for the oxygenated products, most of them were first observed at relatively higher temperatures ( $\geq 978$  K). This finding suggests that these species are not products from the initial oxidation of JP-10 or from initial decomposition intermediates. Ketene (C<sub>2</sub>H<sub>2</sub>O), ethenol (C<sub>2</sub>H<sub>4</sub>O), acetaldehyde (C<sub>2</sub>H<sub>4</sub>O), and ethanol (C<sub>2</sub>H<sub>6</sub>O) define the C2 oxygenated species group. The branching ratios of these species are much lower than the those of C1 and reach only 1.4%. Besides, their appearance temperatures are higher than 978 K. Acetone (C<sub>3</sub>H<sub>6</sub>O) and propanal (C<sub>3</sub>H<sub>6</sub>O) both emerge at 978 K with maximum branching ratios still below 1%. It should be noticed that for the PIE curve of  $m/z = 56$ , a second slope appears at the photon energy of  $10.10 \pm 0.05$  eV, corresponding to the adiabatic photoionization energy of 2-propanal (10.11 eV [50]), indicating the existence of this C3 oxidation product. However, due to the lack of any reference PIE curve of 2-propanal, it is unlikely to reproduce the fit in this work.

Third, furan (C<sub>4</sub>H<sub>4</sub>O), 2-butenal (C<sub>4</sub>H<sub>6</sub>O), and 2,3-dihydrofuran (C<sub>4</sub>H<sub>6</sub>O) represent members of C4 oxygenated specie. 2-butenal and 2,3-dihydrofuran are barely detectable ( $< 0.3\%$ ), but furan represents a significant fraction. Furan, a cyclic ether, is detected at a temperature of 925 K. The branching ratio increase from 1% to 2.7% (951 K) and then drops to 0.4% (1004 K). Based on this trend, we can conclude that furan is likely a key intermediate in the JP-10 oxidation.

Finally, only two C5 oxygenated species were detected: 2,4-cyclopentadiene-1-one (C<sub>5</sub>H<sub>4</sub>O) and 2-cyclopenten-1-one (C<sub>5</sub>H<sub>6</sub>O); both hold only small fractions ( $< 1\%$ ). Considering the C6 oxygenated species phenol (C<sub>6</sub>H<sub>6</sub>O) and 1,2-benzenediol (C<sub>6</sub>H<sub>6</sub>O<sub>2</sub>), their branching ratios are at levels of 2% (951 K); both are initially observed at 925 K suggesting that they might represent products from the oxidation of C6 hydrocarbon intermediates. The remaining oxygenated species are at very low levels of only 0.7%. These are likely products of multiple oxidation reactions with aromatics such as benzene, toluene and naphthalene resulting in low concentration and higher formation temperatures.

## 5. Conclusion

In conclusion, we performed an experimental study on JP-10 oxidation in the flow reactor utilizing the synchrotron vacuum ultraviolet photoionization mass spectrometer method. A comprehensive array of 62 species is identified and quantified, with 25 oxygenated species included. For the hydrocarbon species, the majority are produced and discussed in the pyrolysis of JP-10 without oxygen [42]. Therefore, the yields of the hydrocarbon fragments from JP-10 in the oxidation process are lower than in the pyrolysis of JP-10 in the absence of oxygen. The formation mechanisms of the detected oxygenated species are proposed to be linked to key hydrocarbons detected in the JP-10 pyrolysis. Thus, the oxidation reactions strongly depend on the pyrolysis mechanisms and enhance the pyrolysis processes in return. This

indicates that the oxidation and pyrolysis of JP-10 cannot be uncoupled. Future work will focus on the oxidation of JP-10 at shorter residence times of a few 10  $\mu$ s; further, studies of additives of aluminum nanoparticles are warranted to elucidate the (catalytic) effects of aluminum nanoparticle additives to the reaction mechanism(s) and overall product spectrum.

#### Declaration of Competing Interest

The authors declare that they have no known competing financial interests or personal relationships that could have appeared to influence the work reported in this paper.

#### Acknowledgements

This work was supported by the Office of Naval Research under Contract No. N000141912083.

#### Appendix A. Supplementary data

Supplementary data to this article can be found online at <https://doi.org/10.1016/j.cplett.2020.137490>.

#### References

- [1] N.M. Vandewiele, G.R. Magoon, K.M. Van Geem, M.-F. Reyniers, W.H. Green, G.B. Marin, *Energy Fuels* 28 (2014) 4976–4985.
- [2] H. Li, G. Liu, R. Jiang, L. Wang, X. Zhang, *Combust. Flame* 162 (2015) 2177–2190.
- [3] N.M. Vandewiele, G.R. Magoon, K.M. Van Geem, M.-F. Reyniers, W.H. Green, G.B. Marin, *Energy Fuels* 29 (2014) 413–427.
- [4] L. Yue, H.-J. Xie, X.-M. Qin, X.-X. Lu, W.-J. Fang, *J. Mol. Model.* 19 (2013) 5355–5365.
- [5] K. Chenoweth, A.C.T. van Duin, S. Dasgupta, W.A. Goddard III, *J. Phys. Chem. A* 113 (2009) 1740–1746.
- [6] G.R. Magoon, J. Aguilera-Iparraguirre, W.H. Green, J.J. Lutz, P. Piecuch, H.W. Wong, O.O. Oluwole, *Int. J. Chem. Kinet.* 44 (2012) 179–193.
- [7] J.M. Hudzik, A. Castillo, J.W. Bozzelli, *J. Phys. Chem. A* 119 (2015) 9857–9878.
- [8] K. Wohlwend, L. Maurice, T. Edwards, R. Striebich, M. Vangsness, A. Hill, *J. Propul. Power* 17 (2001) 1258–1262.
- [9] D.W. Mikolaitis, C. Segal, A. Chandy, *J. Propul. Power* 19 (2003) 601–606.
- [10] T.J. Bruno, M.L. Huber, A. Laesecke, E.W. Lemmon, R.A. Perkins, *Tech. Rep. NISTIR 6640* (2006) 325.
- [11] O. Herbinet, B. Sirjean, R. Bounaceur, R. Fournet, F. Battin-Leclerc, G. Scacchi, P.-M. Marquaire, *J. Phys. Chem. A* 110 (2006) 11298–11314.
- [12] S. Nakra, R.J. Green, S.L. Anderson, *Combust. Flame* 144 (2006) 662–674.
- [13] F. Parsinejad, C. Arcari, H. Metghalchi, *Combust. Sci. Technol.* 178 (2006) 975–1000.
- [14] C.Q. Jiao, C.A. DeJoseph, A. Garscadden, *Int. J. Mass Spectrom.* 266 (2007) 92–96.
- [15] Y. Xing, Y.S. Guo, D. Li, W.J. Fang, R.S. Lin, *Energy Fuels* 21 (2007) 1048–1051.
- [16] Y. Xing, W. Fang, W. Xie, Y. Guo, R. Lin, *Ind. Eng. Chem. Res.* 47 (2008) 10034–10040.
- [17] F.J. Yang, Y.S. Guo, Y. Xing, D. Li, W.J. Fang, R.S. Lin, *J. Chem. Eng. Data* 53 (2008) 2237–2240.
- [18] X.H. Su, H.M. Hou, G. Li, R.S. Lin, S.L. Cai, *Acta Chimica Sinica* 67 (2009) 587–592.
- [19] S.H. Park, C.H. Kwon, J. Kim, B.H. Chun, J.W. Kang, J.S. Han, B.H. Jeong, S.H. Kim, *Ind. Eng. Chem. Res.* 49 (2010) 8319–8324.
- [20] M.J. Zehe, R.L. Jaffe, *J. Org. Chem.* 75 (2010) 4387–4391.
- [21] R. Seiser, U. Niemann, K. Seshadri, *Proc. Combust. Inst.* 33 (2011) 1045–1052.
- [22] K.H.H. Goh, P. Geipel, F. Hampf, R.P. Lindstedt, *Proc. Combust. Inst.* 34 (2013) 3311–3318.
- [23] L. Türker, S. Variş, Ç. Çelik Bayar, *Fuel* 104 (2013) 128–132.
- [24] X.M. Qin, H.J. Xie, L. Yue, X.X. Lu, W.J. Fang, *J. Mol. Model.* 20 (2014) 8.
- [25] G. Li, C. Zhang, H. Wei, H. Xie, Y. Guo, W. Fang, *Fuel* 163 (2016) 148–156.
- [26] S. Wang, H.-J. Gou, B.-C. Fan, Y.-Z. He, S.-T. Zhang, J.-P. Cui, *Chin. J. Chem. Phys.* 20 (2007) 48–52.
- [27] C.W. Gao, A.G. Vandeputte, N.W. Yee, W.H. Green, R.E. Bonomi, G.R. Magoon, H.-W. Wong, O.O. Oluwole, D.K. Lewis, N.M. Vandewiele, *Combust. Flame* 162 (2015) 3115–3129.
- [28] F. Guo, X. Cheng, H. Zhang, *Combust. Sci. Technol.* 184 (2012) 1233–1243.
- [29] A.G.G.M. Tielens, *Annu. Rev. Astron. Astrophys.* 46 (2008) 289–337.
- [30] D.F. Davidson, D.C. Horning, J.T. Herbon, R.K. Hanson, *Proc. Combust. Inst.* 28 (2000) 1687–1692.
- [31] M.B. Colket, L.J. Spadaccini, *J. Propul. Power* 17 (2001) 315–323.
- [32] F. Qi, R. Yang, B. Yang, C.Q. Huang, L.X. Wei, J. Wang, L.S. Sheng, Y.W. Zhang, *Rev. Sci. Instrum.* 77 (2006) 084101.
- [33] B. Yang, Y.Y. Li, L.X. Wei, C.Q. Huang, J. Wang, Z.Y. Tian, R. Yang, L.S. Sheng, Y.W. Zhang, F. Qi, *Proc. Combust. Inst.* 31 (2007) 555–563.
- [34] B. Yang, P. Oßwald, Y. Li, J. Wang, L. Wei, Z. Tian, F. Qi, K. Kohse-Höinghaus, *Combust. Flame* 148 (2007) 198–209.
- [35] Y.Y. Li, L.D. Zhang, Z.Y. Tian, T. Yuan, J. Wang, B. Yang, F. Qi, *Energy Fuels* 23 (2009) 1473–1485.
- [36] Y.Y. Li, L.D. Zhang, Z.Y. Tian, T. Yuan, K.W. Zhang, B. Yang, F. Qi, *Proc. Combust. Inst.* 32 (2009) 1293–1300.
- [37] L.D. Zhang, J.H. Cai, T.C. Zhang, F. Qi, *Combust. Flame* 157 (2010) 1686–1697.
- [38] P. Oßwald, H. Güldenbergl, K. Kohse-Höinghaus, B. Yang, T. Yuan, F. Qi, *Combust. Flame* 158 (2011) 2–15.
- [39] F. Qi, *Proc. Combust. Inst.* 34 (2013) 33–63.
- [40] Y. Li, F. Qi, *Acc. Chem. Res.* 43 (2009) 68–78.
- [41] M.F. Russo Jr, A.C. van Duin, *Molecular Dynamics Simulations of Aromatic Hydrocarbon Combustion via the ReaxFF Reactive Force Field*, Abstracts of Papers of the American Chemical Society, American Chemical Society 1155 16th St., NW, Washington, DC 20036 USA (2010).
- [42] L. Zhao, T. Yang, R.I. Kaiser, T.P. Troy, B. Xu, M. Ahmed, J. Alarcon, D. Belisario-Lara, A.M. Mebel, Y. Zhang, *Phys. Chem. Chem. Phys.* 19 (2017) 15780–15807.
- [43] T. Bally, D. Hasselmann, K. Loosen, *Helv. Chim. Acta* 68 (1985) 345–354.
- [44] C. Batich, P. Bischof, E. Heilbronner, *J. Electron Spectrosc. Relat. Phenom.* 1 (1972) 333–353.
- [45] I. Benito, H. Seidl, H. Bock, *Rev. Fac. Cienc. Univ. Oviedo* 14 (1973) 95.
- [46] I. Gotkis, C. Lifshitz, *Org. Mass Spectrom.* 28 (1993) 372–377.
- [47] P.N. Rao, D. Kunzru, *J. Anal. Appl. Pyrolysis* 76 (2006) 154–160.
- [48] R. Striebich, J. Lawrence, *J. Anal. Appl. Pyrolysis* 70 (2003) 339–352.
- [49] J.A. Miller, S.J. Klippenstein, *J. Phys. Chem. A* 107 (2003) 7783–7799.
- [50] T. Adam, R. Zimmermann, *Anal. Bioanal. Chem.* 389 (2007) 1941–1951.